NANO LETTERS

Open Access
This article is licensed under CC-BY-NC-ND 4.0

pubs.acs.org/NanoLett
Letter

Magnetic-Field-Induced Spin Transition in Single-Atom Catalysts for Nitrate Electrolysis to Ammonia

Xingchao You,[#] Zhongyuan Guo,[#] Qiuling Jiang, Junkai Xia, Suwen Wang, Xiaohui Yang, Zechao Zhuang,* Yongfu Li, Hai Xiang, Hao Li,* and Bing Yu*

Cite This: *Nano Lett.* 2025, 25, 8704−8712

Read Online

ACCESS | Metrics & More | Article Recommendations | Supporting Information

ABSTRACT: Electrochemical nitrate reduction (NitRR) using single-atom catalysts (SACs) offers a promising pathway for sustainable ammonia production. Herein, we explore the use of external magnetic fields to regulate the spin state of Ru SACs supported on nitrogen-doped carbon (Ru−N−C), aiming to optimize their catalytic performance toward NitRR. Under magnetic field conditions, Ru−N−C exhibits a remarkable NH_3 yield rate of ∼38 mg L^{-1} h^{-1} and a Faradaic efficiency of ∼95% over 200 h. Our spectroscopic and magnetic characterization demonstrates that the external magnetic field induces a spin transition to a high-spin state in Ru SACs/N−C. Theoretical analysis further suggests that the increased spin state of Ru shifts the density of states away from the Fermi level, weakening the adsorption affinity for *NH_2. Economic analysis hints at cost effectiveness and scalability. Overall, this study demonstrates that magnetic-field-induced spin modulation effectively optimizes NitRR electrocatalysts.

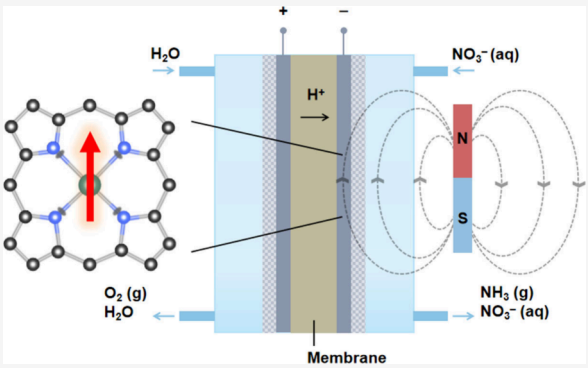

KEYWORDS: *magnetic field, nitrate reduction reaction, ammonia synthesis, spin-state transition, single-atom catalysis*

Electrochemical nitrate reduction to ammonia (NitRR) has emerged as a sustainable method for treating nitrate-rich wastewater.[1−3] Recently, single-atom catalysts (SACs) have garnered significant attention for their ability to catalyze NitRR due to their exceptional atom utilization efficiency, atomic-level structural tunability, and properties that differ substantially from bulk materials.[4,5] Among these, ruthenium (Ru) SACs are particularly notable for their ability to bind and activate various intermediates during NitRR by undergoing changes in oxidation states (commonly ranging from +2 to +4, and even up to +6 or +8).[6,7] To optimize their performance, various strategies for structural modification at single-atom scale have been proposed.[8,9]

Despite the progress made in the synthesis methods, several fundamental challenges associated with NitRR remain unresolved. First, the NitRR process itself is a complex, multistep reaction involving the transfer of eight electrons and nine protons, which intensifies the limitations imposed by linear scaling relationships.[10] Second, certain key steps, such as the hydrogenation of *NO to *NHO, are spin-forbidden,[11] resulting in high kinetic barriers that require spin exchange between intermediates and the catalyst's active sites.

Recent advancements have underscored the potential of external magnetic fields to modulate the spin states of SACs. For example, the application of a mild magnetic field (∼0.5 T) significantly enhances spin-selective charge transfer in a nickel SAC, resulting in a remarkable 2880% increase in oxygen evolution reaction (OER) magnetocurrent.[12] Similarly, a cobalt SAC shows improved OER activity under an alternating magnetic field, driven by spin polarization flips and magnetic heating at the active sites.[13] Additionally, performance enhancement of weakly ferromagnetic iron SACs in the oxygen reduction reaction (ORR) under an external magnetic field has also been demonstrated.[14,15] Although significant progress has been made in applying magnetic fields to modulate SACs for O_2-related reactions, their impact on NitRR, which involves far more electron and proton transfers compared with the OER and ORR, remains largely unexplored.

Herein, for the first time, we propose an effective strategy to apply an external magnetic field to induce spin state regulation of Ru−N−C for NitRR. By using advanced characterization techniques, we prove that the magnetic-field-induced spin transition to a high spin state can optimize the nitrate adsorption. Moreover, our theoretical analysis further reveals that increasing the spin state of Ru shifts the density of states away from the Fermi level. Benefiting from these merits, the Ru−N−C electrocatalyst in the presence of external magnetic

Received: March 14, 2025
Revised: May 8, 2025
Accepted: May 9, 2025
Published: May 14, 2025

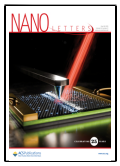

ACS Publications
© 2025 The Authors. Published by American Chemical Society

https://doi.org/10.1021/acs.nanolett.5c01516
Nano Lett. 2025, 25, 8704−8712

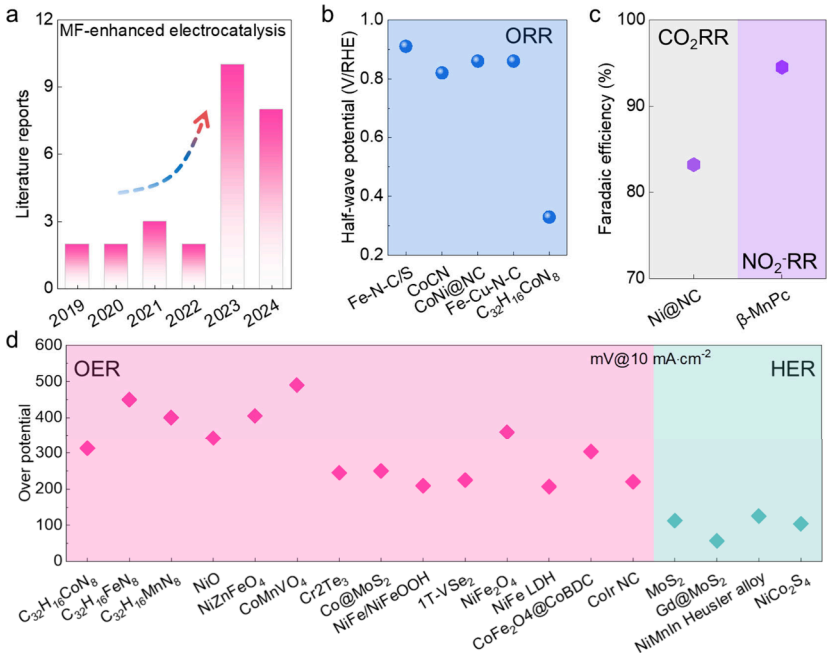

Figure 1. (a) Data mining on the magnetic-field-enhanced electrocatalysis, including (b) the number of closely related literature and improved performance for ORR, (c) the CO_2RR and NO_2^-RR, and (d) the water splitting reactions. All literature data and the corresponding references were extracted via large-scale data mining from the experimental literature published during the past decade, which are also available in the public Digital Catalysis Platform (*DigCat*) database: https://www.digcat.org/.

field demonstrates a remarkable NH_3 yield rate of ~38 mg L^{-1} h^{-1} and a Faradaic efficiency (FE) of ~95% for over 200 h, outperforming that in the absence of external magnetic field.

First, we performed large-scale data mining from the available experimental literature related to magnetic-field-enhanced electrocatalysis, as summarized in Figure 1. It can be clearly seen that, according to the past decade's reports, the magnetic field can change the spin states of active sites and then tune the performance (Figure 1a). For various types of catalysts, with the aid of external magnetic field, the half-wave potential of ORR has been increased (Figure 1b), the Faradaic efficiency of electrochemical CO_2 reduction reaction (CO_2RR) and nitrite reduction reaction (NO_2^-RR) has been improved (Figure 1c), and the overpotential of water splitting reaction has also been deceased (Figure 1d). A detailed summary of these studies on magnetic-field-enhanced electrocatalysis can be found in Tables S1−S3. Based on these findings, we hypothesize that the application of an external magnetic field holds great promise for improving the electrocatalytic performance of materials that contain magnetic properties, especially for those with transition metals as active sites (e.g., SACs).

We synthesized Ru-based catalysts Ru SACs/N−C and Ru NPs/N−C via a one-step pyrolysis of ruthenium chloride, dicyandiamide, and trimesic acid at 900 °C under argon (Figure 2a). Inductively coupled plasma−optical emission spectroscopy (ICP-OES) analysis reveals the Ru loadings in obtained Ru SACs/N−C and Ru NPs/N−C catalysts are 0.18 and 0.56 wt %, respectively. Figure S1a presents a TEM image of the synthesized Ru NPs/N−C, clearly showcasing the nanoparticles dispersed within the N−C substrate. In contrast, the nanoparticles are absent in the TEM image of Ru SACs/N−C.[16,17] Additionally, HAADF-STEM offers compelling evidence for the exclusive presence of Ru SACs dispersed within Ru SACs/N−C (Figure 2b). Further confirmation is provided by elemental mapping (Figure 2c), which verifies the presence of well-dispersed C, N, and Ru elements.[18] To determine the structures more accurately, we performed electron energy loss spectroscopy (EELS) analysis (Figure S2 and the corresponding discussions in the Supporting Information).

XRD patterns of Ru SACs/N−C and Ru NPs/N−C exhibit only two broad diffraction peaks, situated at roughly 26° and 44°. These peaks correspond to (002) and (100) planes of graphitic carbon, respectively (Figure 2d).[19] The absence of distinct peaks supports the formation of single-atom metal sites in Ru SACs/N−C, corroborating the HAADF-STEM findings.[20] At room temperature, no discrete single-line EPR spectrum characteristic of free radicals was detected. Instead, Ru SACs/N−C exhibits a stronger, broad EPR spectrum with a g value of 2.002 (Figure 2e). Previous studies have elucidated that distortions within the p_z orbitals of nitrogen atoms can extend partially into the d_{xy} orbitals, potentially reconfiguring electron localization.[21] Consequently, it is hypothesized that interactions between Ru central atoms and N ligands in Ru SACs/N−C may lead to unique spatial arrangement structures and distinct spin states, resulting in exceptional magnetic characteristics. It is well established that interactions between an unpaired electron and its local environment can significantly affect the shape of the EPR signal peak. In comparison to Ru SACs/N−C, Ru NPs/N−C exhibits a marked attenuation in EPR spectrum, indicating a reduction in the number of unpaired electrons.[22]

Subsequently, the oxidation states of Ru SACs/N−C and Ru NPs/N−C were analyzed by using X-ray photoelectron spectroscopy (XPS). The high-resolution Ru $3p_{3/2}$ spectrum of Ru NPs/N−C exhibits distinct peaks at 460.68, 464.08, 482.68, and 488.88 eV (Figure 2f), indicating the coexistence of Ru^0 and Ru^{3+} states. Conversely, the relatively low Ru loading in Ru SACs/N−C results in very weak signals in the

https://doi.org/10.1021/acs.nanolett.5c01516
Nano Lett. 2025, 25, 8704−8712

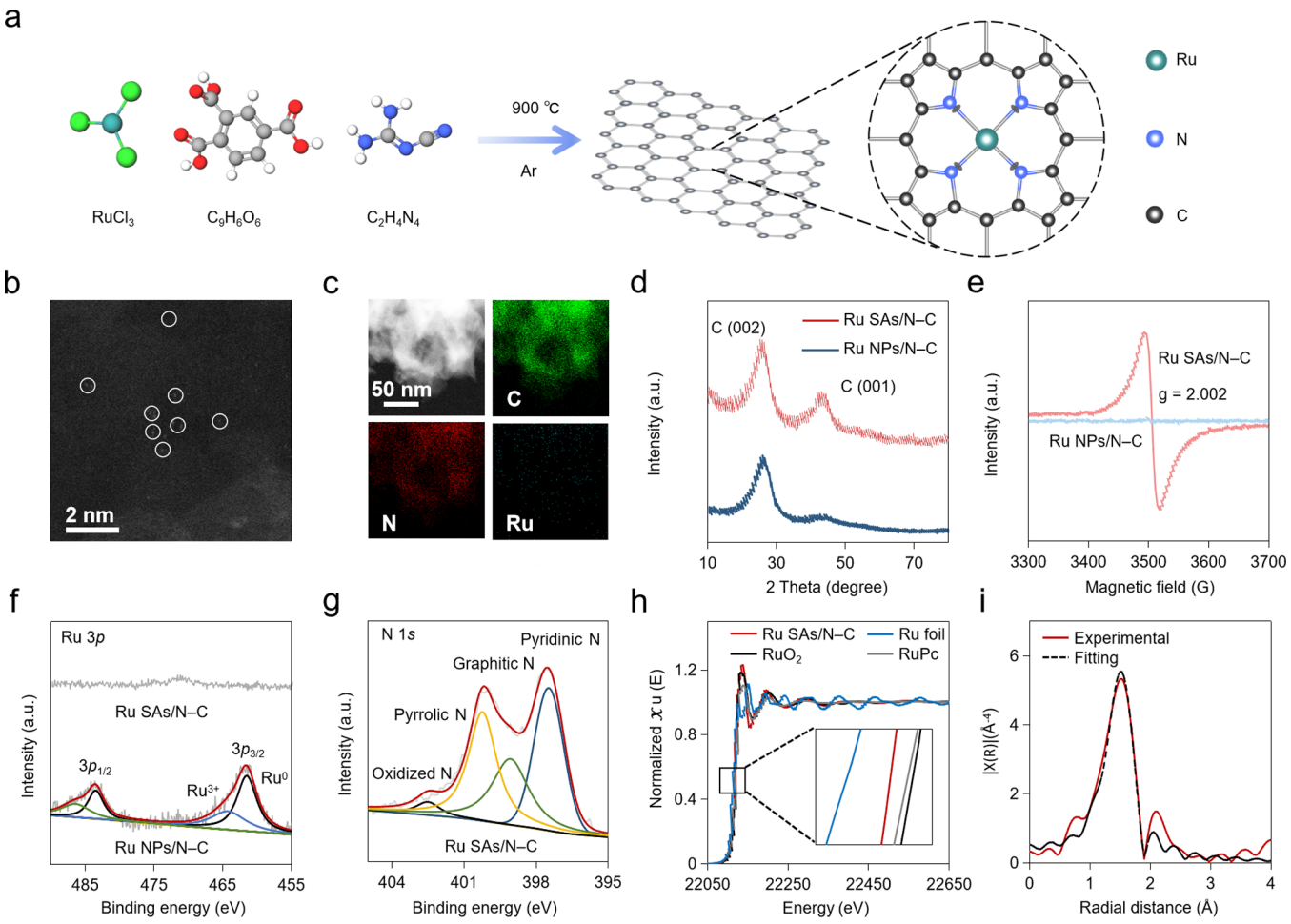

Figure 2. (a) Schematic representation of the synthetic process of Ru SACs/N−C and Ru NPs/N−C catalysts. (b) HAADF-STEM image of Ru SACs/N−C. (c) Elemental mapping of Ru SACs/N−C. (d) XRD patterns of Ru NPs/N−C and Ru SACs/N−C. (e) EPR spectra of Ru NPs/N−C and Ru SACs/N−C. (f) The high-resolution Ru 3p spectra of Ru NPs/N−C and Ru SACs/N−C. (g) The high-resolution N 1s spectra of Ru SACs/N−C. (h) Normalized Ru *K*-edge XANES curves. (i) EXAFS *R*-space fitting curve.

high-resolution Ru 3p spectrum.[23,24] The carbon species in both Ru SACs/N−C and Ru NPs/N−C can be categorized into three types (Figure S3 and the corresponding discussions). The high-resolution O 1s XPS spectra further demonstrate the presence of absorbed O_2 (530.7 eV), C=O (532.2 eV), and C−OH/C−O−OH groups (533.6 eV; Figure S4). Additionally, the N 1s XPS spectra of both Ru SACs/N−C and Ru NPs/N−C reveal the existence of four nitrogen types (Figure S5). Overall, Ru SACs/N−C demonstrates a distinct local electronic structure of Ru compared with Ru NPs/N−C.

X-ray absorption near-edge structure (XANES) and extended X-ray absorption fine structure (EXAFS) analyses were performed to gain a comprehensive understanding of the electronic structure and local coordination environment of the Ru SACs/N−C catalyst. Figure 2h presents the Ru *K*-edge XANES spectra for Ru SACs/N−C, with RuO_2, Ru phthalocyanine (Pc), and Ru foil as reference materials. The Ru *K*-edge XANES spectrum of Ru SACs/N−C shows an absorption edge situated between those of Ru metal foil and RuO_2, indicating that the oxidation state of the single-atom Ru in the catalyst is between Ru^0 and Ru^{4+}.[25] To further elucidate the Ru coordination environment, we performed EXAFS fitting to determine the structural parameters. The fitting results indicate that each Ru atom is coordinated by an average of four nitrogen ligands. Based on these findings, the proposed coordination structure of Ru SACs/N−C is $Ru-N_4$, as illustrated in Figure 2i and the corresponding discussions in the Supporting Information.

To investigate the effect of magnetic fields on the electrochemical performance, we placed a three-electrode system in a magnetic field. Twenty neodymium magnets, each 3 cm × 2 cm × 0.5 cm, were positioned next to the working electrode in a custom H-shaped glass cell, ensuring constant field strength during tests (Figure 3a). The NitRR activities of the prepared catalysts were first tested in a two-compartment H-type electrolytic cell containing 0.1 M K_2SO_4 and 0.0025 M KNO_3 solutions using linear sweep voltammetry (LSV). All potentials were calibrated according to the reversible hydrogen electrode (RHE) scale. A comparison of the polarization curves with and without KNO_3 confirms the occurrence of NitRR (blue and red lines in Figure 3b).[10] In the presence of magnetic field, Ru SACs/N−C exhibits the most significant polarization curve response among all the tested catalysts, suggesting it may possess superior catalytic performance toward NitRR. Subsequent chronoamperometric tests show that Ru SACs/N−C exhibits an increased ammonia yield after the application of magnetic field (Figure 3c), particularly in the range from −0.6 to −0.8 V vs RHE. It can be observed in Figure 3d that Ru NPs/N−C shows a low catalytic

https://doi.org/10.1021/acs.nanolett.5c01516
Nano Lett. 2025, 25, 8704−8712

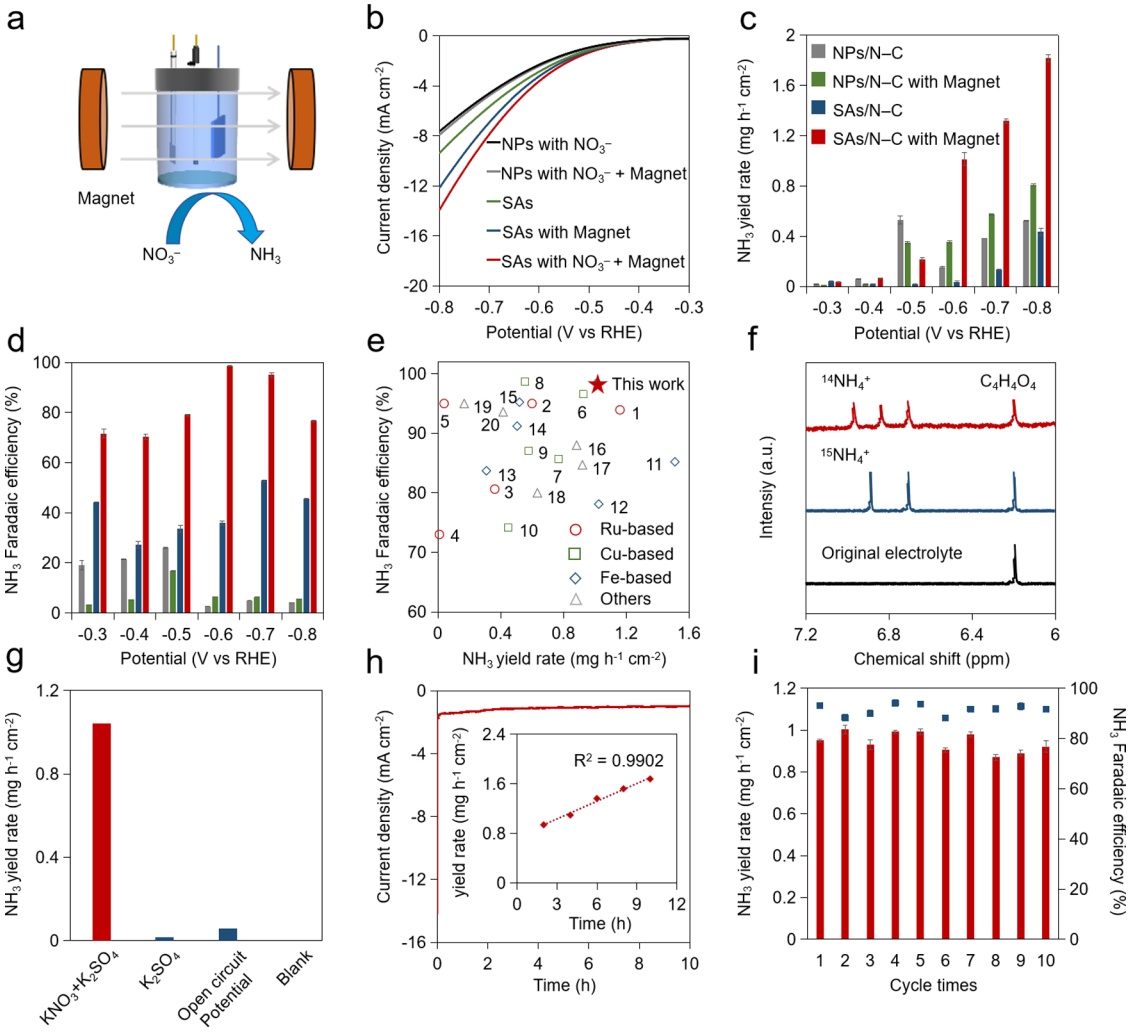

Figure 3. (a) Schematic test equipment of the NitRR under a constant magnetic field. (b) The LSV curves of Ru NPs/N−C in the 0.1 M K_2SO_4 with 2.5 mM KNO_3, Ru NPs/N−C in the 0.1 M K_2SO_4 with 2.5 mM KNO_3 under magnetic field, Ru SACs/N−C in the 0.1 M K_2SO_4, Ru SACs/N−C in the 0.1 M K_2SO_4 under magnetic field, and Ru SACs/N−C in the 0.1 M K_2SO_4 with 2.5 mM KNO_3 under magnetic field. (c) NH_3 yield rates and (d) FEs of Ru NPs/N−C and Ru SACs/N−C at various applied potentials with or without a magnetic field. (e) Comparison of the NH_3 yield rates and FEs of Ru SACs/N−C under a magetic field with other reported electrocatalysts. (f) ^1H NMR spectra of the electrolyte fed by $K^{14}NO_3$ and $K^{15}NO_3$ after NitRR. (g) Comparison of the amount of produced NH_3 under four different conditions. (h) The long-term stability of Ru SACs/N−C with time-dependent current density curve and yield (inset) for the duration of 10 h. (i) Cycling tests of Ru SACs/N−C at −0.6 V vs RHE.

selectivity toward ammonia synthesis, with FE values less than 30% at all tested potentials, no matter in the magnetic environment or not. In contrast, Ru SACs/N−C exhibits significantly higher FEs in the presence of a magnetic environment, with the maximum FE reaching 98.61% at −0.6 V vs RHE. A plausible explanation is that the magnetic field tends to regulate the spin states of SACs and reduce the kinetic barriers of spin-related processes in catalytic reactions, thus enhancing the catalysts' activity and selectivity.[26,27]

The M-H curves of Ru SACs/N−C and Ru NPs/N−C are displayed in Figure S7a. Furthermore, we measured the magnetization intensity as a function of temperature (Figure S7b and the corresponding discussions in the Supporting Information). Combined with the EPR results, this observation suggests the spin states of Ru SACs/N−C undergo changes under the influence of a magnetic field. Compared to other recently reported catalysts, Ru SACs/N−C demonstrates remarkable catalytic advantages at extremely low NO_3^- concentrations under magnetic conditions (Figure 3e).

To determine the nitrogen source in this experimental system, we detected NH_4^+ in the Ru SACs/N−C reaction system through nuclear magnetic resonance (NMR) and comparative experiments. The $^{14}NH_4^+$ generated under different chemical shifts of $^{14}NO_3^-$ appears as a triple nuclear magnetic resonance peak, while the $^{15}NH_4^+$ synthesized from $^{15}NO_3^-$ appears as a double nuclear magnetic resonance peak (Figure 3f).[28] No significant NH_4^+ was detected in the electrolytes of K_2SO_4, open circuit potential, or blank in the control electrolysis experiments. The ammonia yield detected in the K_2SO_4 solution containing KNO_3 was determined by using the indophenol blue method, and the results are consistent with those presented in Figure 3c. The above results confirm the nitrogen source of NH_4^+ is NO_3^-, rather than other substances in the environmental system.[8]

The stability of a catalyst is crucial when evaluating its performance.[29] The current density of Ru SACs/N−C remains constant during 10 h of continuous electrolysis, and the ammonia production exhibits good time dependence (Figure

https://doi.org/10.1021/acs.nanolett.5c01516
Nano Lett. 2025, 25, 8704−8712

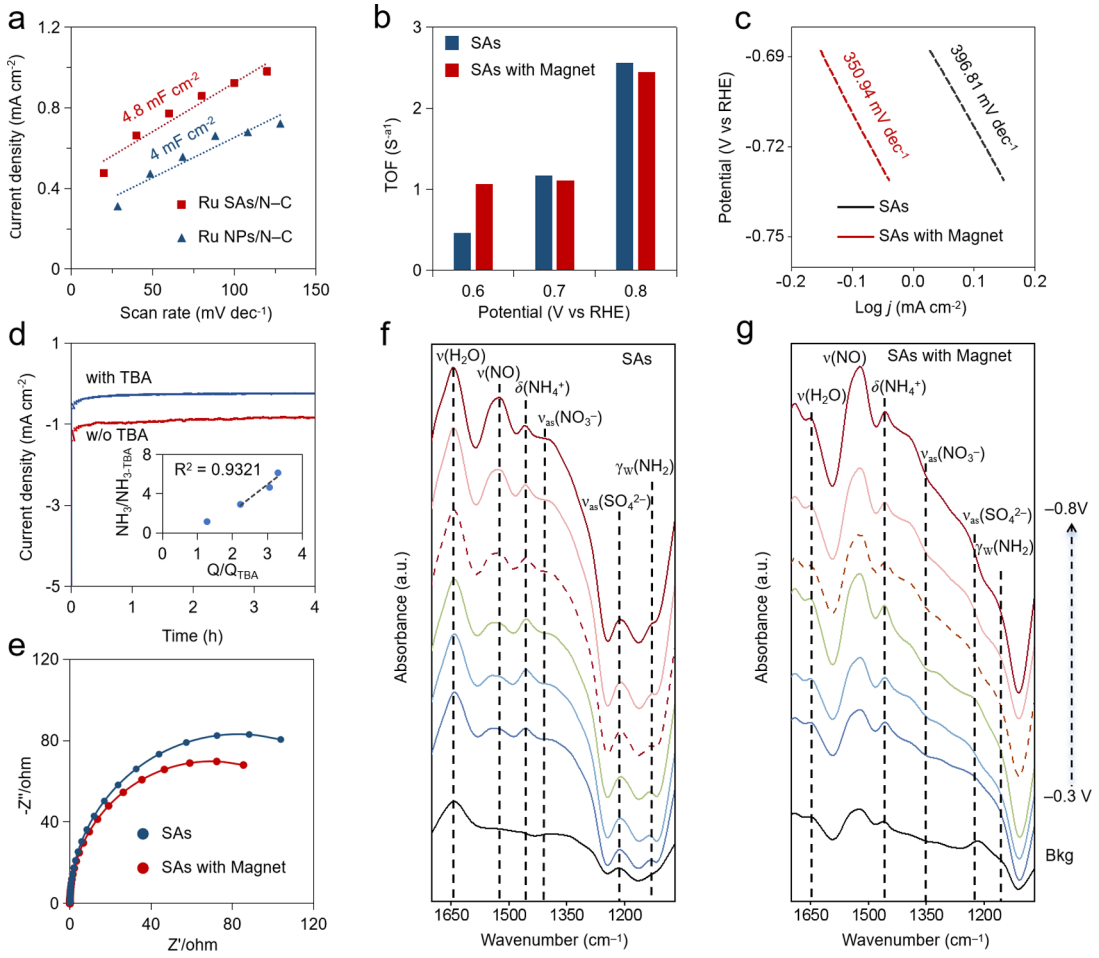

Figure 4. (a) C_{dl} values of Ru SACs/N−C with and without a magnetic field. (b) TOFs of Ru SACs/N−C at different potentitals with and without magnetic field. (c) Tafel slopes for the Ru SACs/N−C electrodes in 0.1 M K_2SO_4 electrolyte containing 0.0025 M nitrate with and without a magnetic field. (d) The relationship between Q/Q_{TBA} and $NH_3/NH_{3\text{-}TBA}$ ratios. (e) Electrochemical intensity spectra of Ru SACs/N−C with and without magnetic field. (f) Potential-dependent *in situ* ATR-FTIR spectra of the electroreduction process. (g) Potential-dependent *in situ* ATR-FTIR spectra of the electroreduction process with a magnetic field.

3h). After the electrolysis was completed, we tested the cycling stability of the catalyst when changing the electrolyte, and Ru SACs/N−C still maintained satisfactory stability (Figure 3i).

To elucidate the catalytic mechanism of Ru SACs/N−C in the NitRR under an external magnetic field, we conducted more electrochemical measurements and *in situ* characterizations. First, the electrochemically active surface areas (ECSA) of Ru SACs/N−C under both magnetic and nonmagnetic conditions were compared using the double-layer capacitance (C_{dl}) method (Figure 4a and Figure S8). The results show the C_{dl} value of Ru SACs/N−C increases significantly from 4.0 to 4.8 mF cm^{-2} upon the magnetic field, indicating the magnetic field effectively activated the active sites.[30] Simultaneously, the turnover frequency (TOF) of Ru SACs/N−C under the magnetic field is significantly higher (1.061 s^{-1}) than without the magnetic field (0.464 s^{-1}; Figure 4b), demonstrating the magnetic field effectively enhances the intrinsic activity of the catalyst.[31] Subsequently, the Tafel slope analysis further reveals the impact of the magnetic field on the NitRR kinetics. Compared with the nonmagnetic conditions (396.81 mV dec^{-1}), Ru SACs/N−C under magnetic field exhibits a smaller Tafel slope (350.94 mV dec^{-1}), which can be attributed to the spin state regulation induced by the magnetic field (Figure 4c). This regulation promotes the orbital interaction between active sites and reaction intermediates, thus reducing the reaction barrier and leading to better NitRR kinetics.[32]

To investigate the role of active hydrogen species, *tert*-butanol (TBA) was introduced as a hydrogen radical scavenger.[33] As shown in Figure 4d, the ammonia yield decreases gradually with the increasing concentration of TBA, indicating that TBA effectively suppresses the •H pathway involved in the Ru SACs/N−C catalyzed NitRR. Furthermore, both the current efficiency (J) and total charge (Q) of the Ru SACs/N−C-based NitRR process are lower when TBA is added compared to the case without TBA (Figure 4d). Additionally, we plotted the relationship between the total charge ratio (Q/Q_{TBA}) and the ammonia yield ratio ($NH_3/NH_{3\text{-}TBA}$) at different reaction times (inset of Figure 4d). The results show that in the initial stage of the reaction (1 h), Q/Q_{TBA} is only 1.15, while $NH_3/NH_{3\text{-}TBA}$ reaches 1.27, suggesting a rapid •H-mediated pathway for the conversion of nitrate to ammonia. The reaction of TBA with •H inhibits the contribution of •H to the ammonia generation in NitRR. Notably, a linear correlation (R^2 = 0.9321) is observed between the ratio of $NH_3/NH_{3\text{-}TBA}$ and Q/Q_{TBA} with reaction time, indicating hydrogenation and electron transfer play a more crucial role in the later stages of NitRR.[34] On the other

https://doi.org/10.1021/acs.nanolett.5c01516
Nano Lett. 2025, 25, 8704−8712

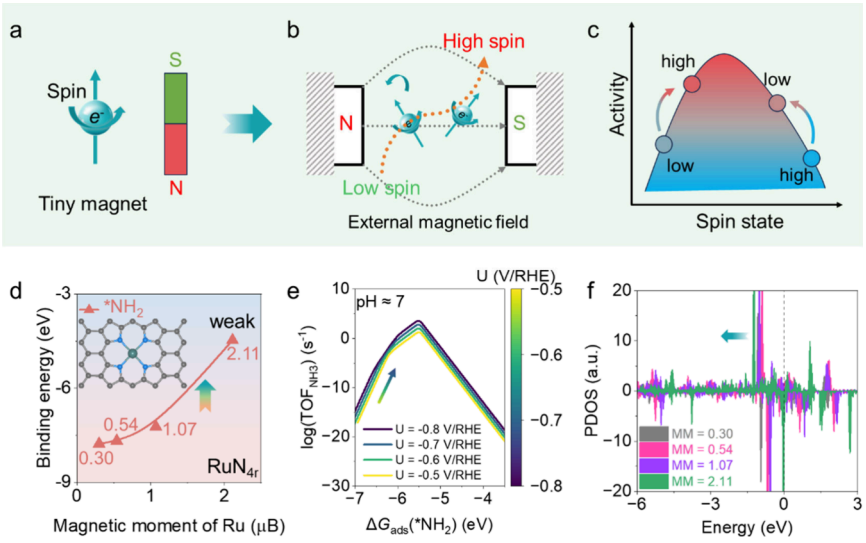

Figure 5. Mechanism behind the external magnetic field to enhance the electrochemical NitRR. (a) Schematic diagram of spinning electrons acting as tiny magnets. (b) Generation of polarized electrons under an external magnetic field. (c) The relationship between the spin state of metal sites and their delivered activity. (d) The binding energy of $*NH_2$ on single-atom Ru supported by the pyrrolic-N environment (inserted structure) at various magnetic moments. (e) The derived pH-dependent activity volcano plot for the electrochemical NO_3^- reduction. (f) PDOS of Ru at various magnetic moment levels.

hand, electrochemical impedance spectroscopy (EIS) shows the charge transfer resistance (R_{ct}) at the electrolyte/electrode interface of Ru SACs/N−C decreases under a magnetic field (Figure 4e), suggesting that the magnetic field facilitates charge transfer.[35]

In situ attenuated total reflection Fourier transform infrared (ATR-FTIR) spectroscopy was employed to characterize potential intermediates in the reaction system (Figure 4f). As the applied potential is swept from open circuit potential to −0.8 V vs RHE, the intensity of negative vibrational band associated with $*NO_3$ (~1400 cm^{-1}) gradually increases, indicating the continuous consumption of nitrate during the NitRR process.[36] Concurrently, multiple peaks emerge at increasingly negative potentials, corresponding to the deoxygenated intermediate (*NO at 1540 cm^{-1})[36] and the hydrogenated intermediate ($*NH_2$ at 1130 cm^{-1}).[37] These observations suggest that the Ru SACs/N−C NitRR process generates abundant deoxygenated/hydrogenated intermediates that ultimately convert to NH_4^+. The presence of $*NH_2$ at ~1130 cm^{-1} further confirms the spin transition from a low-spin state to a high-spin state necessary for the hydrogenation process. Under an external magnetic field, the intensity of the negative vibrational band associated with $*NO_3$ (~1350 cm^{-1}) increases with increasing voltage (Figure 4g), and the signal of the deoxygenated intermediate (*NO at 1520 cm^{-1}) is significantly stronger compared to that without a magnetic field, indicating the external magnetic field induces spin transition to a high-spin state in Ru SACs/N−C, which optimizes nitrate adsorption and promotes electron transfer from the *NO intermediate.[38] The O−H bending vibration of H_2O (around 1650 cm^{-1}) gradually intensified from −0.3 to −0.8 V vs RHE, suggesting the involvement of H_2O in the Ru SACs/N−C-based NitRR process.[39] Combining the data shown in Figures 4f and 4g, it is clear that Ru SACs/N−C is highly efficient in dissociating H_2O to generate abundant $^•H$ species.

To further illustrate the origin of the external magnetic field in enhancing the performance of NitRR over Ru SACs/N−C, we studied the effect of spin states on the adsorption of the key intermediate, i.e., $*NH_2$, pH-dependent reaction activity, and the electronic structure. As a SAC material, RuN_{4r} with the pyrrolic-N coordination environment in the Ru SACs/N−C configuration can deliver a precise platform to uncover the spin effect of active sites induced by the magnetic field on the electrochemical performance compared to polyatomic or cluster catalysts. As for the spinning electron, it can act like a tiny magnet, which generates a magnetic field around itself (Figure 5a). When Ru SACs are put into an external magnetic field, the polarized electrons will generate, leading to the transition from low spin to high spin states (Figure 5b). Changing the spin state can significantly affect catalytic activity by altering the binding imteraction with adsorbates according to the previous studies.[40−44] Therefore, tuning the spin state of active sites is a good strategy to control the reaction activity (Figure 5c).

In a previous mechanistic study on electrochemical NitRR, we derived a pH-dependent activity volcano model at the RHE scale by considering the effects of pH, electric field, linear scaling relations, and the potential of zero charges, which has been deployed in the *DigCat* platform for public users.[45] The model study shows that the adsorption strength of the $*NH_2$ inermediate is a key descriptor to describe the reaction performance of NitRR. Therefore, based on the RuN_{4r} model built, we show using density function theory (DFT) calculations that the spin state of single-site Ru has a substantial effect on the adsorption of $*NH_2$, and the adsorption of $*NH_2$ is shown to be the strongest on the low-spin polarized ground state Ru site (0.30 μB) (Figure 5d). Under an external magnetic field, the electronic structure of Ru will transit to a higher spin state, weakening the adsorption strength of $*NH_2$. According to the pH-dependent volcano model (Figure 5e), we can find that the weakened adsorption of $*NH_2$ intermediates in the magnetic field will boost the reaction activity of the NitRR close to the volcano peak, which is in good agreement with our experimental observations. Furthermore, the analysis of the electronic structure for single-

https://doi.org/10.1021/acs.nanolett.5c01516
Nano Lett. 2025, 25, 8704−8712

site Ru suggests the origin of how the spin state of single-site Ru determines the binding strength of *NH_2 (Figure 5f). The density of states (DOS) analysis shows that with the increase of the spin state on Ru, the distribution of DOS shifts toward to the negative energy level, away from the Fermi level, suggesting that there would be more electrons occupying on the antibonding orbital when Ru interacting with *NH_2 species. Therefore, the high spin state of Ru reduces the adsorption affinity for *NH_2, thereby altering the behavior of the NitRR.

Finally, we explored the practical application potential of Ru SACs/N−C for NitRR (Figures S9 and S10 and the corresponding discussions in the Supporting Information). Ru SACs/N−C demonstrates robust nitrate reduction performance (~98% FE) across varying nitrate concentrations and competing ions. Long-term stability tests in a flow cell (200 h at 100 mA cm^{-2}) confirm its practical potential, achieving ~95% FE and 38 mg L^{-1} h^{-1} of NH_3 yield. Economic analysis reveals that scaling up current densities (>400 mA cm^{-2}) could reduce NH_3 production costs below commercial prices ($1.0−1.5 kg^{-1}), highlighting its viability for sustainable nitrate removal despite current cost challenges.

In summary, we propose an effective strategy to apply external magnetic fields for inducing the spin state regulation of Ru SACs/N−C in nitrate reduction. Experimental and theoretical studies reveal that an external magnetic field induces a spin transition to a high spin state in Ru SACs/N−C, which promotes the hydrogeneration of *NO to *NHO and weakens *NH_2 adsorption. Overall, our work provides a promising approach for improving electrocatalytic performance through magnetic-field-induced spin state modulation, offering valuable insights for the development of efficient and sustainable electrochemical technologies for ammonia production and wastewater treatment.

■ ASSOCIATED CONTENT

Supporting Information

The Supporting Information is available free of charge at https://pubs.acs.org/doi/10.1021/acs.nanolett.5c01516.

Experimental section; TEM images; XPS spectra; electron energy-loss spectra, M-H curves, FT-EXAFS spectra and the corresponding wavelet transform analysis; NitRR results under various environmental conditions; durability−time plot of the Ru SACs/N−C operating in a membrane electrode; and economic assessment results (PDF)

■ AUTHOR INFORMATION

Corresponding Authors

Zechao Zhuang − *Department of Chemistry, Tsinghua University, Beijing 100084, China*; Email: zhuangzc@mail.tsinghua.edu.cn

Hao Li − *Advanced Institute for Materials Research (WPI-AIMR), Tohoku University, Sendai 980-8577, Japan*; orcid.org/0000-0002-7577-1366; Email: li.hao.b8@tohoku.ac.jp

Bing Yu − *National Key Laboratory for Development and Utilization of Forest Food Resources, Zhejiang A&F University, Hangzhou 311300, China; Ecological-Environment & Health College (EEHC), Zhejiang A&F University, Hangzhou 311300, China*; orcid.org/0000-0001-6468-8578; Email: bing.yu@zafu.edu.cn

Authors

Xingchao You − *National Key Laboratory for Development and Utilization of Forest Food Resources, Zhejiang A&F University, Hangzhou 311300, China; Ecological-Environment & Health College (EEHC), Zhejiang A&F University, Hangzhou 311300, China*

Zhongyuan Guo − *Advanced Institute for Materials Research (WPI-AIMR), Tohoku University, Sendai 980-8577, Japan; College of Environmental and Resource Sciences, Zhejiang University, Hangzhou 310058, China*

Qiuling Jiang − *Advanced Institute for Materials Research (WPI-AIMR), Tohoku University, Sendai 980-8577, Japan*

Junkai Xia − *National Key Laboratory for Development and Utilization of Forest Food Resources, Zhejiang A&F University, Hangzhou 311300, China; Ecological-Environment & Health College (EEHC), Zhejiang A&F University, Hangzhou 311300, China*

Suwen Wang − *National Key Laboratory for Development and Utilization of Forest Food Resources, Zhejiang A&F University, Hangzhou 311300, China; Ecological-Environment & Health College (EEHC), Zhejiang A&F University, Hangzhou 311300, China*

Xiaohui Yang − *National Key Laboratory for Development and Utilization of Forest Food Resources, Zhejiang A&F University, Hangzhou 311300, China; Ecological-Environment & Health College (EEHC), Zhejiang A&F University, Hangzhou 311300, China*

Yongfu Li − *National Key Laboratory for Development and Utilization of Forest Food Resources, Zhejiang A&F University, Hangzhou 311300, China; Ecological-Environment & Health College (EEHC), Zhejiang A&F University, Hangzhou 311300, China*

Hai Xiang − *National Key Laboratory for Development and Utilization of Forest Food Resources, Zhejiang A&F University, Hangzhou 311300, China; Ecological-Environment & Health College (EEHC), Zhejiang A&F University, Hangzhou 311300, China*

Complete contact information is available at: https://pubs.acs.org/10.1021/acs.nanolett.5c01516

Author Contributions

#X.C.Y. and Z.G. contributed equally to this work.

Notes

The authors declare no competing financial interest.

■ ACKNOWLEDGMENTS

This work was supported financially by the Key Research and Development Project of Science and Technology Department of Zhejiang Province (2023C02019; 2025C2096), the National Natural Science Foundation of China (22006018), the National Key Research and Development Program of China (2022YFE0127800), the Talent Starting-Up Project of Research Development Fund of Zhejiang A&F University (2034020103), the JSPS KAKENHI (JP25K01737), and the Postdoctoral Fellowship Program of CPSF under Grant GZC20241472. H.L. acknowledges the Center for Computational Materials Science, Institute for Materials Research, Tohoku University for the use of MASAMUNE-IMR (202412-SCKXX-0211), and the Institute for Solid State Physics (ISSP) at the University of Tokyo for the use of their supercomputers.

https://doi.org/10.1021/acs.nanolett.5c01516
Nano Lett. 2025, 25, 8704−8712

REFERENCES

(1) Han, S.; Li, H.; Li, T.; Chen, F.; Yang, R.; Yu, Y.; Zhang, B. Ultralow overpotential nitrate reduction to ammonia via a three-step relay mechanism. *Nat. Catal.* **2023**, *6* (5), 402−414.

(2) Zhang, G.; Li, B.; Shi, Y.; Zhou, Q.; Fu, W.-J.; Zhou, G.; Ma, J.; Yin, S.; Yuan, W.; Miao, S.; et al. Ammonia recovery from nitrate-rich wastewater using a membrane-free electrochemical system. *Nat. Sustain.* **2024**, *7* (10), 1251−1263.

(3) Li, P.; Li, R.; Liu, Y.; Xie, M.; Jin, Z.; Yu, G. Pulsed nitrate-to-ammonia electroreduction facilitated by tandem catalysis of nitrite intermediates. *J. Am. Chem. Soc.* **2023**, *145* (11), 6471−6479.

(4) Xu, J.; Zhang, S.; Liu, H.; Liu, S.; Yuan, Y.; Meng, Y.; Wang, M.; Shen, C.; Peng, Q.; Chen, J.; et al. Breaking local charge symmetry of iron single atoms for efficient electrocatalytic nitrate reduction to ammonia. *Angew. Chem., Int. Ed.* **2023**, *62* (39), No. e202308044.

(5) Liang, J.; Li, J.; Dong, H.; Li, Z.; He, X.; Wang, Y.; Yao, Y.; Ren, Y.; Sun, S.; Luo, Y.; et al. Aqueous alternating electrolysis prolongs electrode lifespans under harsh operation conditions. *Nat. Commun.* **2024**, *15* (1), 6208.

(6) Xiang, T.; Liu, X.; Wang, Z.; Zeng, Y.; Deng, J.; Xiong, W.; Cheng, M.; Liu, J.; Zhou, C.; Yang, Y. Boosting active hydrogen generation via ruthenium single atoms for efficient electrocatalytic nitrate reduction to ammonia. *Appl. Catal. B-Environ* **2025**, *365*, 124943.

(7) Chen, F.-Y.; Wu, Z.-Y.; Gupta, S.; Rivera, D. J.; Lambeets, S. V.; Pecaut, S.; Kim, J. Y. T.; Zhu, P.; Finfrock, Y. Z.; Meira, D. M.; et al. Efficient conversion of low-concentration nitrate sources into ammonia on a Ru-dispersed Cu nanowire electrocatalyst. *Nat. Nanotechnol.* **2022**, *17* (7), 759−767.

(8) Xia, J.; Xu, J.; Yu, B.; Liang, X.; Qiu, Z.; Li, H.; Feng, H.; Li, Y.; Cai, Y.; Wei, H.; et al. A metal-sulfur-carbon catalyst mimicking the two-component architecture of nitrogenase. *Angew. Chem., Int. Ed.* **2024**, *136* (45), No. e202412740.

(9) Yang, M.; Li, B.; Li, S.; Dong, Q.; Huang, Z.; Zheng, S.; Fang, Y.; Zhou, G.; Chen, X.; Zhu, X.; et al. Highly selective electrochemical nitrate to ammonia conversion by dispersed Ru in a multielement alloy catalyst. *Nano Lett.* **2023**, *23* (16), 7733−7742.

(10) Wang, S.; Zhuang, Z.; Xu, J.; Fu, C.; Qiu, Z.; Feng, H.; Xiang, H.; Chen, Z.; Li, H.; Zhang, L.; et al. Non-rigid metal-oxygen bonding empowered nitrate reduction on ruthenium catalysts. *Nano Energy* **2024**, *130*, 110088.

(11) Janaway, G. A.; Brauman, J. I. Direct observation of spin forbidden proton-transfer reactions: $^{3}NO^{-}$ + HA → ^{1}HNO + A^{-}. *J. Phys. Chem. A* **2000**, *104* (9), 1795−1798.

(12) Zhu, H.; Sun, S.; Hao, J.; Zhuang, Z.; Zhang, S.; Wang, T.; Kang, Q.; Lu, S.; Wang, X.; Lai, F.; et al. A high-entropy atomic environment converts inactive to active sites for electrocatalysis. *Energy. Environ. Sci.* **2023**, *16* (2), 619−628.

(13) Gong, X.; Jiang, Z.; Zeng, W.; Hu, C.; Luo, X.; Lei, W.; Yuan, C. Alternating magnetic field induced magnetic heating in ferromagnetic cobalt single-atom catalysts for efficient oxygen evolution reaction. *Nano Lett.* **2022**, *22* (23), 9411−9417.

(14) Kiciński, W.; Sęk, J. P.; Matysiak-Brynda, E.; Miecznikowski, K.; Donten, M.; Budner, B.; Nowicka, A. M. Enhancement of PGM-free oxygen reduction electrocatalyst performance for conventional and enzymatic fuel cells: The influence of an external magnetic field. *Appl. Catal., B* **2019**, *258*, 117955.

(15) Bayaguud, A.; Fu, Y.; Zhu, C. Interfacial parasitic reactions of zinc anodes in zinc ion batteries: underestimated corrosion and hydrogen evolution reactions and their suppression strategies. *J. Energy Chem.* **2022**, *64*, 246−262.

(16) Chen, W.; Yu, M.; Liu, S.; Zhang, C.; Jiang, S.; Duan, G. Recent progress of Ru single-atom catalyst: synthesis, modification, and energetic applications. *Adv. Funct. Mater.* **2024**, *34*, 2313307.

(17) Cui, Z.; Ren, Z.; Ma, C.; Chen, B.; Chen, G.; Lu, R.; Zhu, W.; Gan, T.; Wang, Z.; Zhuang, Z.; et al. Dilute RuCo alloy synergizing single Ru and Co atoms as efficient and CO-resistant anode catalyst for anion exchange membrane fuel cells. *Angew. Chem., Int. Ed.* **2024**, No. e202404761.

(18) Sun, J.-F.; Xu, Q.-Q.; Qi, J.-L.; Zhou, D.; Zhu, H.-Y.; Yin, J.-Z. Isolated single atoms anchored on N-doped carbon materials as a highly efficient catalyst for electrochemical and organic reactions. *ACS Sustain. Chem. Eng.* **2020**, *8* (39), 14630−14656.

(19) Wang, Y.; Meng, P.; Yang, Z.; Jiang, M.; Yang, J.; Li, H.; Zhang, J.; Sun, B.; Fu, C. Regulation of atomic Fe-spin state by crystal field and magnetic field for enhanced oxygen electrocatalysis in rechargeable zinc-air batteries. *Angew. Chem., Int. Ed.* **2023**, *62* (28), No. e202304229.

(20) Yu, J.; Wang, A.; Yu, W.; Liu, X.; Li, X.; Liu, H.; Hu, Y.; Wu, Y.; Zhou, W. Tailoring the ruthenium reactive sites on N doped molybdenum carbide nanosheets via the anti-ostwald ripening as efficient electrocatalyst for hydrogen evolution reaction in alkaline media. *Appl. Catal., B* **2020**, *277*, 119236.

(21) Galardon, E.; Le Maux, P.; Paul, C.; Poriel, C.; Simonneaux, G. ^{1}H-NMR and EPR studies of the electronic structure of low-spin ruthenium (III) isocyanide porphyrin complexes: unusual $(dxz, dyz)^{4}$ $(dxy)^{1}$ configuration. *J. Organomet. Chem.* **2001**, *629* (1−2), 145−152.

(22) Zhang, J.; Zhao, Y.; Zhao, W.; Wang, J.; Hu, Y.; Huang, C.; Zou, X.; Liu, Y.; Zhang, D.; Lu, X.; et al. Improving electrocatalytic oxygen evolution through local field distortion in Mg/Fe dual-site catalysts. *Angew. Chem., Int. Ed.* **2023**, *62* (52), No. e202314303.

(23) Liu, R.; Sun, M.; Liu, X.; Lv, Z.; Yu, X.; Wang, J.; Liu, Y.; Li, L.; Feng, X.; Yang, W.; et al. Enhanced metal-support interactions boost the electrocatalytic water splitting of supported ruthenium nanoparticles on a Ni_3N/NiO heterojunction at industrial current density. *Angew. Chem., Int. Ed.* **2023**, *62* (46), No. e202312644.

(24) Liu, Z.; Du, Y.; Yu, R.; Zheng, M.; Hu, R.; Wu, J.; Xia, Y.; Zhuang, Z.; Wang, D. Tuning mass transport in electrocatalysis down to sub-5 nm through nanoscale grade separation. *Angew. Chem., Int. Ed.* **2023**, *62* (3), No. e202212653.

(25) Zhao, S.; Hung, S.-F.; Deng, L.; Zeng, W.-J.; Xiao, T.; Li, S.; Kuo, C.-H.; Chen, H.-Y.; Hu, F.; Peng, S. Constructing regulable supports via non-stoichiometric engineering to stabilize ruthenium nanoparticles for enhanced pH-universal water splitting. *Nat. Commun.* **2024**, *15* (1), 2728.

(26) Sun, T.; Tang, Z.; Zang, W.; Li, Z.; Li, J.; Li, Z.; Cao, L.; Dominic Rodriguez, J. S.; Mariano, C. O. M.; Xu, H. Ferromagnetic single-atom spin catalyst for boosting water splitting. *Nat. Nanotechnol.* **2023**, *18* (7), 763−771.

(27) Liu, H.; Jiang, Y.; Li, Q.; Hai, G.; Gu, C.; Du, Y. Interface-triggered spin-magnetic effect in rare earth intraparticle heterostructured nanoalloys for boosting hydrogen evolution. *Angew. Chem., Int. Ed.* **2024**, *63*, No. e202412591.

(28) Wang, S.; Song, C.; Cai, Y.; Li, Y.; Jiang, P.; Li, H.; Yu, B.; Ma, T. Interfacial polarization triggered by covalent-bonded MXene and black Phosphorus for Enhanced Electrochemical Nitrate to ammonia conversion. *Adv. Energy Mater.* **2023**, *13* (31), 2301136.

(29) Spöri, C.; Kwan, J. T. H.; Bonakdarpour, A.; Wilkinson, D. P.; Strasser, P. The stability challenges of oxygen evolving catalysts: towards a common fundamental understanding and mitigation of catalyst degradation. *Angew. Chem., Int. Ed.* **2017**, *56* (22), 5994−6021.

(30) Ma, Y.; Zhou, Y.; Wang, C.; Gao, B.; Li, J.; Zhu, M.; Wu, H.; Zhang, C.; Qin, Y. Photothermal-magnetic synergistic effects in an electrocatalyst for efficient water splitting under optical-magnetic fields. *Adv. Mater.* **2023**, *35* (41), 2303741.

(31) Wu, T.; Ren, X.; Sun, Y.; Sun, S.; Xian, G.; Scherer, G. G.; Fisher, A. C.; Mandler, D.; Ager, J. W.; Grimaud, A.; et al. Spin pinning effect to reconstructed oxyhydroxide layer on ferromagnetic oxides for enhanced water oxidation. *Nat. Commun.* **2021**, *12* (1), 3634.

(32) Ren, X.; Wu, T.; Sun, Y.; Li, Y.; Xian, G.; Liu, X.; Shen, C.; Gracia, J.; Gao, H.-J.; Yang, H.; et al. Spin-polarized oxygen evolution reaction under magnetic field. *Nat. Commun.* **2021**, *12* (1), 2608.

(33) Zhang, J.; Zhang, G.; Lan, H.; Qu, J.; Liu, H. Synergetic hydroxyl radical oxidation with atomic hydrogen reduction lowers the

https://doi.org/10.1021/acs.nanolett.5c01516
Nano Lett. 2025, 25, 8704−8712

organochlorine conversion barrier and potentiates effective contaminant mineralization. *Environ. Sci. Technol.* **2021**, *55* (5), 3296−3304.
(34) Xue, Y.; Yu, Q.; Ma, Q.; Chen, Y.; Zhang, C.; Teng, W.; Fan, J.; Zhang, W.-x. Electrocatalytic hydrogenation boosts reduction of nitrate to ammonia over single-atom Cu with Cu (I)-N_3C_1 sites. *Environ. Sci. Technol.* **2022**, *56* (20), 14797−14807.
(35) Zhou, G.; Wang, P.; Li, H.; Hu, B.; Sun, Y.; Huang, R.; Liu, L. Spin-state reconfiguration induced by alternating magnetic field for efficient oxygen evolution reaction. *Nat. Commun.* **2021**, *12* (1), 4827.
(36) Arana, J.; Garzon Sousa, D.; Gonzalez Diaz, O.; Pulido Melian, E.; Dona Rodriguez, J.M. Effect of NO_2 and NO_3^-/HNO_3 adsorption on NO photocatalytic conversion. *Appl. Catal., B* **2019**, *244*, 660−670.
(37) Amores, J. G.; Escribano, V. S.; Ramis, G.; Busca, G. An FT-IR study of ammonia adsorption and oxidation over anatase-supported metal oxides. *Appl. Catal. B-Environ* **1997**, *13* (1), 45−58.
(38) Zhao, X.; Jiang, Y.; Wang, M.; Liu, S.; Wang, Z.; Qian, T.; Yan, C. Optimizing intermediate adsorption via heteroatom ensemble effect over RuFe bimetallic alloy for enhanced nitrate electroreduction to ammonia. *Adv. Energy Mater.* **2023**, *13* (31), 2301409.
(39) Yu, S.; Dong, X.; Zhao, P.; Luo, Z.; Sun, Z.; Yang, X.; Li, Q.; Wang, L.; Zhang, Y.; Zhou, H. Decoupled temperature and pressure hydrothermal synthesis of carbon sub-micron spheres from cellulose. *Nat. Commun.* **2022**, *13* (1), 3616.
(40) Cao, A.; Nørskov, J. K. Spin effects in chemisorption and catalysis. *ACS Catal.* **2023**, *13* (6), 3456−3462.
(41) Cao, A.; Bukas, V. J.; Shadravan, V.; Wang, Z.; Li, H.; Kibsgaard, J.; Chorkendorff, I.; Nørskov, J. K. A spin promotion effect in catalytic ammonia synthesis. *Nat. Commun.* **2022**, *13* (1), 2382.
(42) Dang, Q.; Tang, S.; Liu, T.; Li, X.; Wang, X.; Zhong, W.; Luo, Y.; Jiang, J. Regulating electronic spin moments of single-atom catalyst sites via single-atom promoter tuning on S-vacancy MoS_2 for efficient nitrogen fixation. *J. Phys. Chem. Lett.* **2021**, *12* (34), 8355−8362.
(43) Sun, Y.; Sun, S.; Yang, H.; Xi, S.; Gracia, J.; Xu, Z. J. Spin-related electron transfer and orbital interactions in oxygen electrocatalysis. *Adv. Mater.* **2020**, *32* (39), 2003297.
(44) Wei, X.; Song, S.; Cai, W.; Luo, X.; Jiao, L.; Fang, Q.; Wang, X.; Wu, N.; Luo, Z.; Wang, H.; et al. Tuning the spin state of Fe single atoms by Pd nanoclusters enables robust oxygen reduction with dissociative pathway. *Chem.* **2023**, *9* (1), 181−197.
(45) Zhang, D.; Li, H. Digital catalysis platform (DigCat): a gateway to big data and AI-powered innovations in catalysis. *ChemRxiv* **2024**, DOI: 10.26434/chemrxiv-2024-9lpb9.

https://doi.org/10.1021/acs.nanolett.5c01516
Nano Lett. 2025, 25, 8704−8712